

Design of a noncontact spherical bearing based on near-field acoustic levitation

Journal of Intelligent Material Systems and Structures
2014, Vol. 25(6) 755–767
© The Author(s) 2013
Reprints and permissions:
sagepub.co.uk/journalsPermissions.nav
DOI: 10.1177/1045389X13512903
jim.sagepub.com


Chao Chen, Junshan Wang, Bing Jia and Fan Li

Abstract

Based on near-field acoustic levitation, a noncontact bearing with a spherical rotor was proposed to explore its potential application for novel supporting bearing of suspended gyro. The stator of the noncontact bearing has a hollow bowl-shaped configuration, in order to produce acoustic levitation force for a spherical object. Two orthogonal flexural standing waves were piezoelectrically generated and led to a traveling wave in the stator, and then the induced high-intensity sound in the air gap between the stator and spherical rotor could apply levitation force and even driving force for the spherical rotor. In this article, finite element model of a bowl-shaped piezoelectric stator was built, and the dynamic analysis and parametric optimization for the stator have been conducted. The prototypes were manufactured and vibration parameters of the stators were experimentally obtained. The test system for the noncontact spherical bearing was built, and its levitation and driving characteristics were measured. The spherical rotor successfully achieved levitation and non-contact rotation based on near-field acoustic levitation and the experimental results preliminarily indicate the feasibility of near-field acoustic levitation for suspended gyro.

Keywords

Ultrasonic motor, spherical bearing, acoustic levitation, suspended gyro

Introduction

Mechanical rotor gyros are inherently suited for autonomous navigation systems due to its unique advantages, such as multi-axis measurement, attitude sensitivity without any external information, no radiation of any internal information, and strong anti-interference. As a key supporting structure, bearings may result in considerable friction torques on the mechanical rotor and even affect the position precision of rotational gyroscopes (Frazier et al., 1974). The conventional bearings have gradually become a limiting factor in the performance of framework gyroscope due to frictional heat and disturbing friction. In this case, various types of noncontact bearings using magnetic field or electric field have been thoroughly studied to reduce disturbing torques on rotational gyroscopes with levitating rotor. By means of magnetic or electrostatic suspension, gyroscope rotor can obtain high speed. Despite an excellent performance, complex and high-cost equipment is desirable for both electric and magnetic suspension (Higuchi et al., 1984; Huxley et al., 1987; Titterton and Weston, 1997), and the inferior cost performance is determined by their inherent characteristics. For example, electrostatic suspension requires high vacuum to avoid electric

breakdown in the case of strong electric field, and strong magnetic field, which may affect the performance of electric instruments in systems, is applied for magnetic levitation. Moreover, the levitated object must be made from special materials with electromagnetic properties. In this case, it seems to be difficult for both electric and magnetic suspension to be wildly applied in navigation and directional fixture.

In order to explore a kind of potential suspension mechanism for rotational gyroscopes, a noncontact spherical bearing based on near-field acoustic levitation (NFAL) is proposed here. NFAL has been expected to be an interesting alternative for near frictionless operation of high-precision machinery and noncontact transportation. NFAL phenomenon occurs when an object close to a vibrating surface is levitated in the near-field

State Key Laboratory of Mechanics and Control for Mechanical Structures, Nanjing University of Aeronautics and Astronautics, Nanjing, China

Corresponding author:

Chao Chen, State Key Laboratory of Mechanics and Control for Mechanical Structures, Nanjing University of Aeronautics and Astronautics, Nanjing 210016, China.
Email: chaochen@nuaa.edu.cn

by the acoustic radiation in the air gap (Chu and Apfel, 1982; Lee and Wang, 1993). Acoustic radiation force is considered as a static force, and the plane object hovers a short distance above the vibrating plate when the acoustic radiation force and the weight of the plane object are in equilibrium. Hashimoto et al. (1995) prove that planar heavy objects of 10 kg weight can be levitated in the near-field region by the acoustic radiation force without any reflector. The deformation of the radiator changes the boundary condition of gas squeeze film, and the calculated levitation force considering vibrator surface displacement distribution is more realistic and fits better with experimentally measured levitation force (Liu et al., 2009; Zhao and Wallaschek, 2011). With an excited flexural traveling wave along the vibrating plate, acoustic streaming is generated in the same direction as the traveling wave in the air gap between the levitated object and the vibrating plate. Due to the acoustic viscous force, the object can be transported without contact (Hashimoto et al., 1998; Hu et al., 2003; Minikes and Bucher, 2003; Ueha et al., 2000). Several kinds of levitated stage based on NFAL are reported for noncontact bearing of precise position (Koyama et al., 2007; Stolarski, 2010; Ide et al., 2005, 2007). In these studies, a noncontact stage using special topology design, that is, square, V or \wedge section shapes beam, is proposed to obtain stable, precise, and virtually frictionless support and actuation. A novel self-levitating journal bearing is presented and has potential for practical applications where required load capacity is low but operating environment demands absolute cleanliness, compact design, and energy efficiency. Experimental results provide conclusive proof that the concept of a journal bearing utilizing acoustic levitation is feasible (Stolarski et al., 2011; Zhao and Wallaschek, 2012). And NFAL is applicable to noncontact rotation ultrasonic motors by means of generated traveling wave in the circumferential direction (Hu et al., 1997; Yamayoshi et al., 1994, 1996; Zhao, 2010). Due to its levitation mechanism, noncontact rotation ultrasonic motors are suitable for small, long-life, and high-speed motors. By appropriate topology structure applying NFAL mechanism, stable levitation can be obtained, which is basic element for suspending gyroscopes. Moreover, high-speed rotation of the levitated rotor may be achieved by means of acoustic streaming when a flexural traveling wave is generated along the vibrating structure. As we know, reaction forces of other physical fields, for example, electric or magnetic field, can also be applied to drive the suspended gyrorotor based on acoustic levitation. By all appearances, compact size and low cost will be obtained for gyroscopes only based on NFAL mechanism.

In this article, a spherical bearing design idea using bowl-shaped noncontact ultrasonic motor is presented to provide a potential application to noncontact support for levitation gyroscopes, requiring neither special

materials for the rotatory rotor nor complicated levitation control. By means of appropriate dynamic design, excited standing or flexural traveling waves on the vibrating stator surface produce a load-carrying squeeze film, which can levitate or even directly drive spherical rotor to rotate without contact. Finally, the prototypes were manufactured, and its levitation and propulsion characteristics were experimentally investigated.

Noncontact spherical bearing and operation principle

As a noncontact bearing, levitation characteristics, including levitation stability and rigidity, have a good effect on anti-interference performance of suspending gyros. In this article, levitation ability of spherical rotor applying NFAL mechanism is investigated. Moreover, rotation characteristics are also analyzed experimentally, because NFAL may provide both levitation and drive force for suspending rotational gyroscopes. Figure 1 illustrates the concept of a noncontact ultrasonic motor with spherical rotor. The noncontact ultrasonic motor, which can form a spherical bearing of inertial device with suspending gyrorotor, has the geometry of a spherical sound radiation surface, in order to produce an air gap between the vibration surface and spherical rotor. A piezoceramic ring is bonded to the stator and has the function of exciting two standing waves with both temporal and phase difference of 90°. The piezoceramic ring is divided into two groups indicated by A and B, which consists of sectors of different polarizations. Figure 2 illustrates that the polarization directions in each sectors are identified by alternating signs. Each sector corresponds to a quarter of the wavelength of the working mode excited in the stator, and this arrangement of polarization determines that the stator only vibrates in several specific mode shapes. In order to increase the vibrating amplitudes of the stator, we may choose the low resonant frequency. Figure 3 shows that two orthogonal working modes denoted by A and B have four nodal diameters along the circumferential direction. Two orthogonal modes with the same eigenfrequency can be excited by A and B groups of piezoelectric elements, respectively, as shown in Figure 2. We assume that two standing waves be expressed as

$$\begin{aligned} \mathbf{A} : u_1(x, t) &= 2U_1 \sin kx \cos \omega t \\ &= U_1 \sin(kx - \omega t) + U_1 \sin(kx + \omega t) \end{aligned} \quad (1)$$

$$\begin{aligned} \mathbf{B} : u_2(x, t) &= 2U_2 \sin k(x + \alpha) \cos(\omega t + \beta) \\ &= U_2 \sin[k(x + \alpha) - (\omega t + \beta)] \\ &\quad + U_2 \sin[k(x + \alpha) + (\omega t + \beta)] \end{aligned} \quad (2)$$

where U_1 and U_2 are the amplitudes, k is the wave number, ω is the circular frequency, and α and β are phase differences in space and time, respectively. Taking

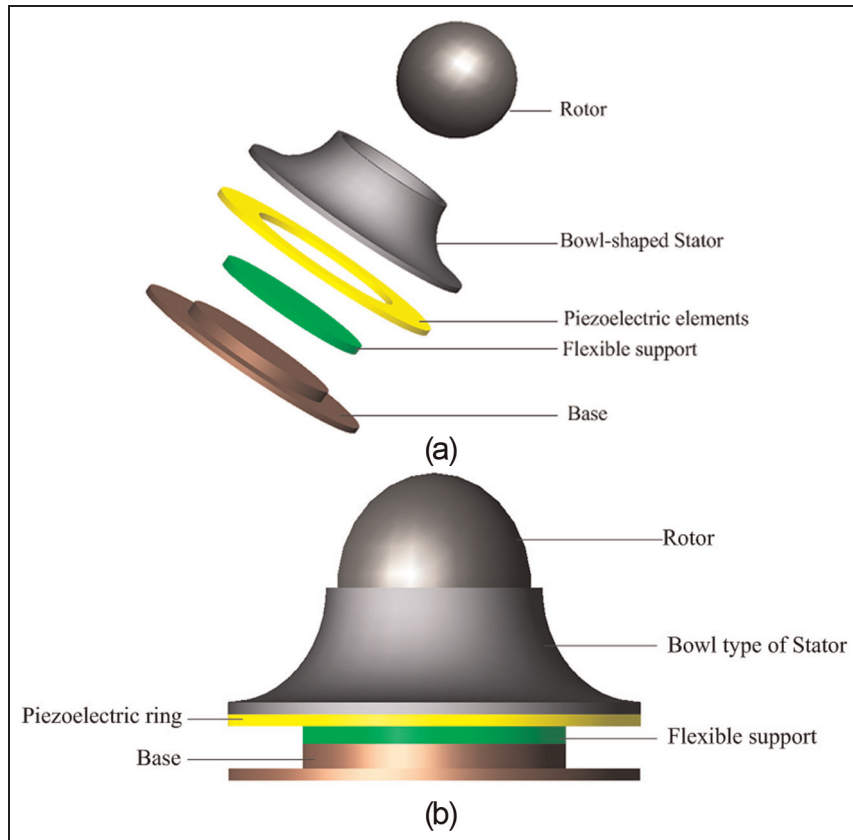


Figure 1. Noncontact spherical bearing using bowl type of ultrasonic motor: (a) exploded view and (b) assembling drawing.

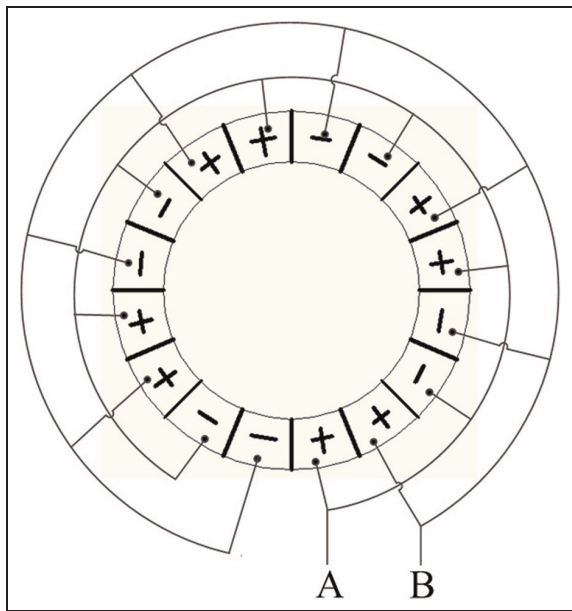


Figure 2. Polarization and disposal of the circular piezoelectric ceramics.

Signs "+" and "−" denote polarization in the adverse direction.

$(k\alpha - \beta) = \varphi_1$ and $(k\alpha + \beta) = \varphi_2$, equation (2) can be changed into

$$\begin{aligned} B : u_2(x, t) &= U_2 \sin(kx + \varphi_1 - \omega t) \\ &+ U_2 \sin(kx + \varphi_2 + \omega t) \end{aligned} \quad (3)$$

When the elastic body is excited by two lead zirconate titanate (PZT) groups denoted by A and B, two standing waves can be produced synchronously. Superposition of the two standing waves may lead to a traveling wave. Taking the summation of equations (1) and (3), we obtain a composing wave. Then the conditions of exciting a traveling wave are

$$\begin{cases} \varphi_1 = k\alpha - \beta = m\pi, & m = \pm 0, \pm 2, \pm 4, \dots \\ \varphi_2 = k\alpha + \beta = n\pi, & n = \pm 1, \pm 3, \pm 5, \dots \\ 2k\alpha = (m + n)\pi & \alpha = \lambda(m + n)/4 \\ \beta = \pi(n - m)/2 \end{cases} \quad (4)$$

Substituting φ_1 and φ_2 into equation (3) and combining equation (1) with equation (3) yield

$$\begin{aligned} u(x, t) &= U_1 \sin(kx - \omega t) + U_1 \sin(kx + \omega t) \\ &+ U_2 \sin(kx + m\pi - \omega t) + U_2 \sin(kx + n\pi + \omega t) \\ &= (U_1 + U_2) \sin(kx - \omega t) + (U_1 - U_2) \sin(kx + \omega t) \end{aligned} \quad (5)$$

When $U_1 = U_2 = U$, the traveling wave can be expressed as

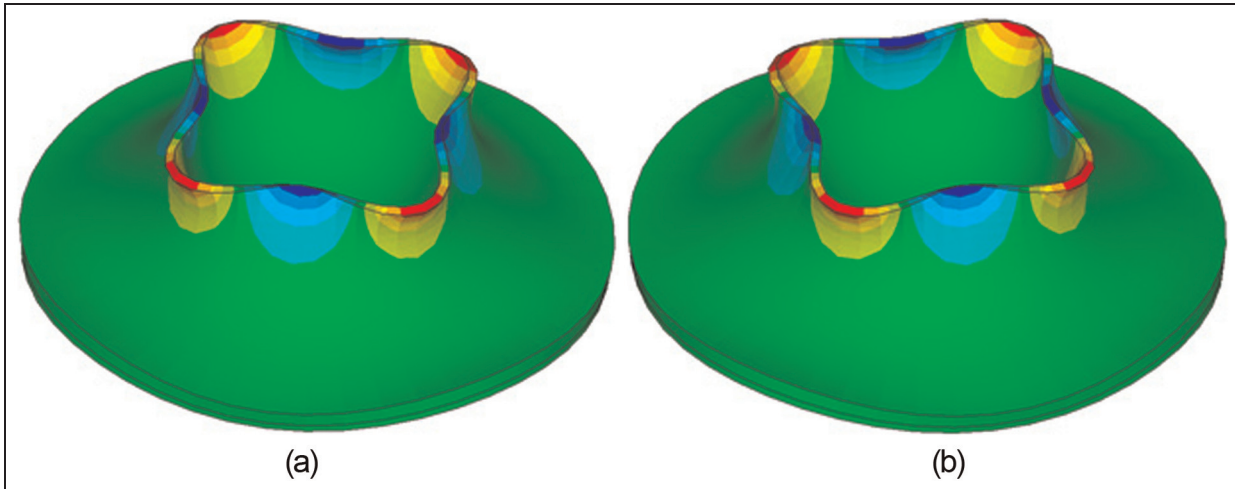


Figure 3. Working modes of bowl-shaped stator: (a) Mode A and (b) Mode B.

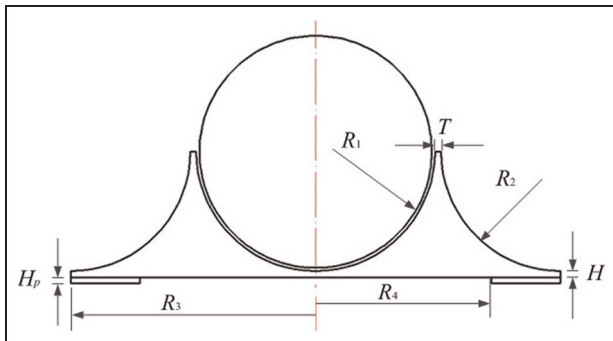


Figure 4. Design parameters of bowl-shaped stator.

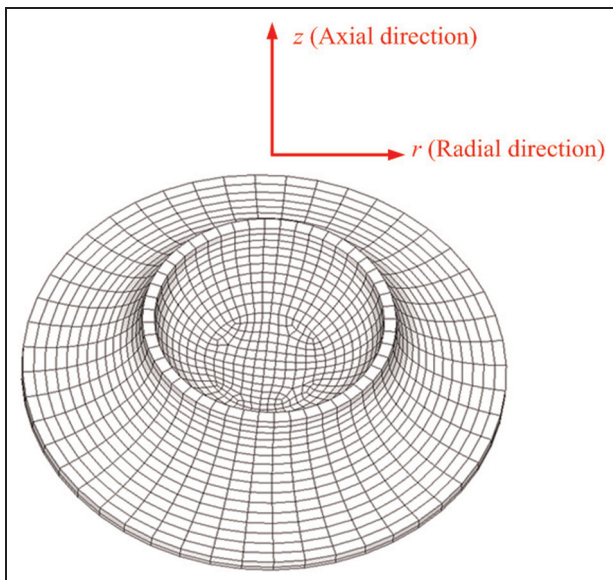


Figure 5. Finite element model of bowl-shaped stator.

$$u(x, t) = 2U \sin(kx - \omega t) \quad (6)$$

Therefore, the conditions exciting the traveling wave in the elastic stator shown in equation (4) become

$$\begin{cases} \alpha = \lambda(n + m)/4 \\ \beta = \pi(n - m)/2 \\ U_1 = U_2 = U \end{cases} \quad (7)$$

When $m = 0$ and $n = 1$, two high-frequency voltages with a temporal phase shift of 90° are applied to A and B groups of piezoelectric elements simultaneously, the two working modes generated are interfered mutually and the result is a traveling wave at the spherical surface of the stator, permitting both the levitation and rotary propulsion of the spherical rotor by means of an air gap.

Parametric design of bowl-shaped stator

The levitation ability of the air gap applied on the rotor depends on the stator vibration, because the sound field induced in the air gap results from the displacements of the surface points located on the stator. A high levitation rigidity and high-speed rotation of the spherical rotor can be obtained when traveling wave with appropriate vibration parameters in the stator is generated. Figure 4 illustrates the bowl-shaped stator profile with the design parameters to be determined.

In addition to the defined radius of the spherical rotor, R_1 , the selected PZT ring purchased from HAIYING Enterprise Group Co., Ltd, has the inner and outer diameters of 40 and 28 mm, respectively, and the height of 0.5 mm. Moreover, with the defined material, the stator vibration mostly depends on R_2 , H , and T . ANSYS software is applied to simulate the dynamic response of the bowl-shaped stator actuated by PZT ring. Figure 5 shows the finite element model of the stator.

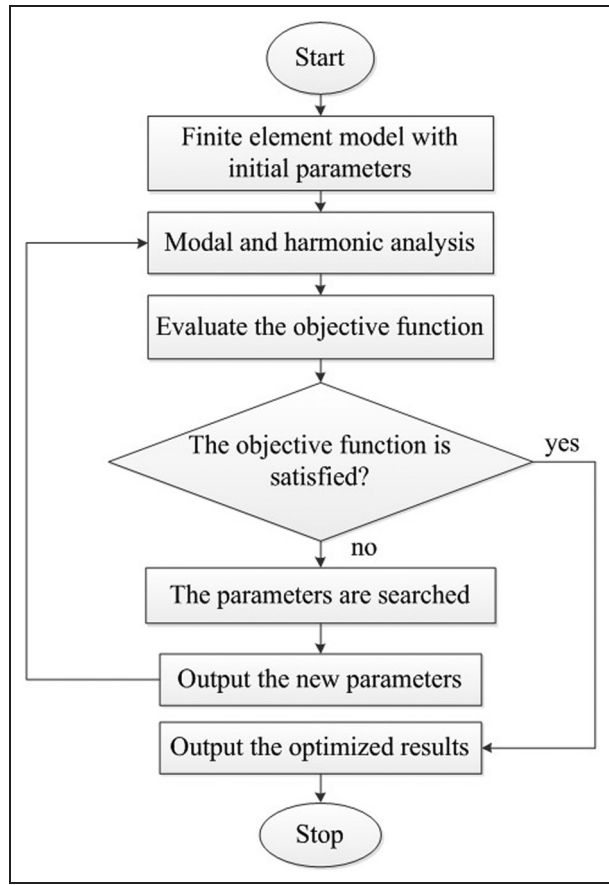


Figure 6. Flow chart of parameter optimization.

Table I. Duralumin for bowl-shaped stator.

Material	Density (kg/m ³)	Elastic modulus (10 ¹⁰ N/m ²)	Poisson ratio
Duralumin	2740	7.17	0.33

Although the precise expression for dynamic mechanism of near-field acoustic field has been still a challenging problem needed to be solved, the classic formulas, no matter Rayleigh radiation pressure equation, or Langevin radiation pressure equation denote that both amplitude and frequency of vibrating surface have effect on real acoustic radiation pressure. Furthermore, Chu and Apfel (1982) deduce the improved formula of acoustic radiation pressure by vibrating piston and also denote the contribution of amplitude and frequency of vibrating surface. In this case, acoustic radiation pressure can be approximately evaluated by the bowl-shaped stator. With the larger product of vibration amplitude and frequency of the stator, a strong acoustic field may occur in the air gap. As shown in Figure 3, large vibration displacement happens on the top of the stator. So the vibration

response of the points here has remarkable effect on the rotary spherical rotor. We define the objective function just as equation (8), which can approximately describe the contribution of the stator vibration to the induced sound field

$$F_{obj} = \frac{1}{fA} \quad (8)$$

where f is vibration frequency of the stator, and A is the radial amplitude of the points on the top of the bowl-shaped stator.

Therefore, the mathematical model for optimal design of the stator is a minimization problem as follows

$$\text{MIN } F_{obj}(R_2, H, T) = \frac{1}{fA} \quad (9)$$

The optimal calculation is carried out in ANSYS, and its flow chart is shown in Figure 6. The stator material is duralumin, whose parameters are listed in Table 1.

The applied piezoelectric ceramic, PZT 8, has the following physical parameters

$$\rho = 7600 \text{ kg m}^{-3} \quad (10)$$

$$[\epsilon] = \begin{bmatrix} 7.124 & & \\ & 7.124 & \\ & & 5.841 \end{bmatrix} \times 10^{-9} \text{ F/m} \quad (11)$$

$$[e] = \begin{bmatrix} 0 & 0 & -5.2 \\ 0 & 0 & -5.2 \\ 0 & 0 & 15.1 \\ 0 & 0 & 0 \\ 0 & 12.7 & 0 \\ 12.7 & 0 & 0 \end{bmatrix} \text{ C/m}^2 \quad (12)$$

$$[C] = \begin{bmatrix} 12.06 & 5.35 & 5.15 & 0 & 0 & 0 \\ 5.35 & 12.06 & 5.15 & 0 & 0 & 0 \\ 5.15 & 5.15 & 10.45 & 0 & 0 & 0 \\ 0 & 0 & 0 & 3.13 & 0 & 0 \\ 0 & 0 & 0 & 0 & 3.13 & 0 \\ 0 & 0 & 0 & 0 & 0 & 3.46 \end{bmatrix} \times 10^{10} \text{ N/m}^2 \quad (13)$$

The initial and optimization dimensions of the stator are listed in Table 2. Based on the optimal parameters, the stator's modal frequency with four 4 waves (see Figure 3) is 51 kHz, and the calculated radial amplitude is 1.5 μm with the applied voltages of 100 V_{pp}. The iteration processes of the design parameters and objective function are shown in Figure 7.

Experiments

Modal tests of the stator

In Figure 8, the manufactured prototypes, which apply the optimal and initial parameters in Table 2, are

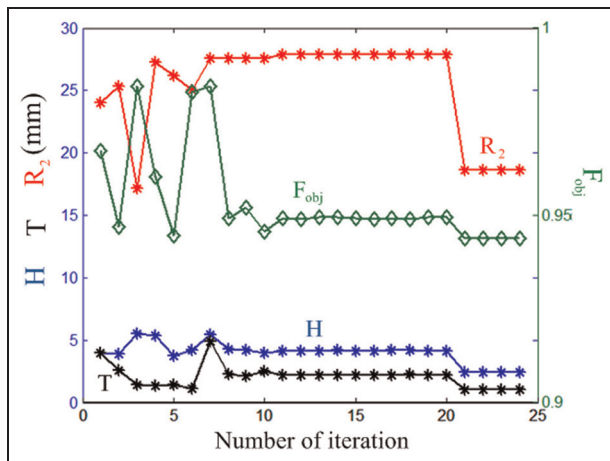


Figure 7. Iteration procedure of design parameters and objection function.

identified by I and II, respectively. Figure 9 also illustrates a series of hemisphere shells made of duralumin to form the rotor. The hemispherical shells with the same external diameter and different masses are fabricated to analyze experimentally the levitation characteristics of the noncontact ultrasonic motor. Two groups of piezoelectric elements denoted by A and B are glued on the bottom of the stator, as shown in Figure 10.

Figure 11 illustrates the Laser Doppler Measurement System (PSV-300F-B; Polytec Ltd, Germany) applied for noncontact measurement, visualization, and analysis of structural vibrations of the stator. Figure 12 shows the frequency response of stator I measured by Laser Doppler Measurement System (PSV-300F). The working modes can be excited by applying voltage signals at working frequencies to group A or group B in the stators (see Figure 10). Figure 13 shows the measured axial displacement response on the top surface of the stator, that is, modal shape. The red and green areas denote inverse displacement in the axial direction, respectively, and the displacement amplitude of $0.4 \mu\text{m}$ was experimentally obtained. Moreover, we measured the radial vibration response of some different points on the lateral surface of the stator. It is found that the radial amplitude of the stator reached about $1.4 \mu\text{m}$. Figure 14 shows the measured point with maximal radial displacement. In the same way, the modal response of stator II with the initial parameters can also be experimentally obtained. The detailed results are listed in Table 3. We



Figure 8. Bowl-shaped stators: stators I and II applying optimal and initial parameters, respectively.

note that the better vibration response is obtained for stator I applying optimal parameters.

Levitation characteristics experiment

Applying input voltages on the piezoelectric ring, vibration response of B_4 mode will induce the acoustic field, and the resulting sound radiation pressure in the air gap will push the rotor to levitate. Figure 15 illustrates that the experimental setup for the levitation characteristics of the presented noncontact ultrasonic actuator includes a high-accuracy Laser Displacement Sensor (Keyence LK-G30, only for single measurement), charge-coupled device (CCD) controller, power amplifier and data acquisition and process module. We defined one point on the rotor surface and measured its displacement response by the sensor, as shown in Figure 16. In this case, a laser beam from LK-G30 irradiates the observed point on the edge of the hemispherical rotor surface, and levitation distance of the rotor can be probed by measuring vertical displacement response.

With piezoelectric vibration in the bowl type of stator, the hemispherical rotor of the prototype can be levitated by the induced acoustic force. Figure 17 illustrates the time history of vertical displacement of the rotor, which indicates the levitation height. We have experimentally obtained levitation characteristics of the noncontact ultrasonic motors with stator I or II, respectively. First, a voltage of 260 V at frequency of 52.06 kHz is applied to stator I, and the measured displacement in the vertical direction indicates the levitation height of the rotors, as shown in Figure 17. It is

Table 2. Initial and optimal parameters of the stator.

	R_1 (mm)	R_2 (mm)	R_3 (mm)	R_4 (mm)	T (mm)	H (mm)	H_p
Initial parameters	19	24	40	28	4	4	I
Optimal parameters	19	18.65	40	28	1.02	2.41	I

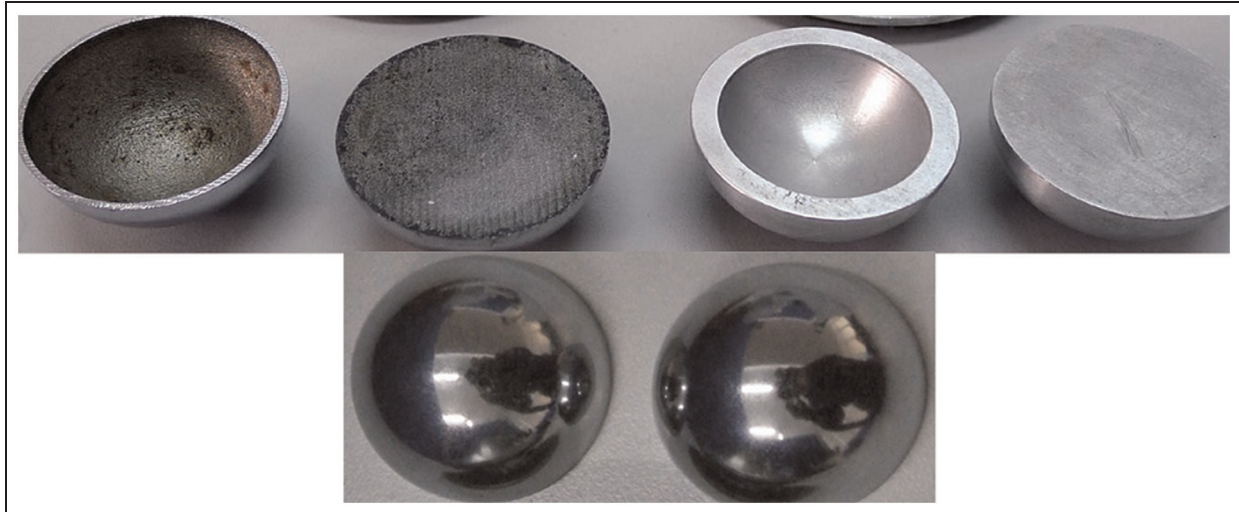


Figure 9. Hemispherical rotors.

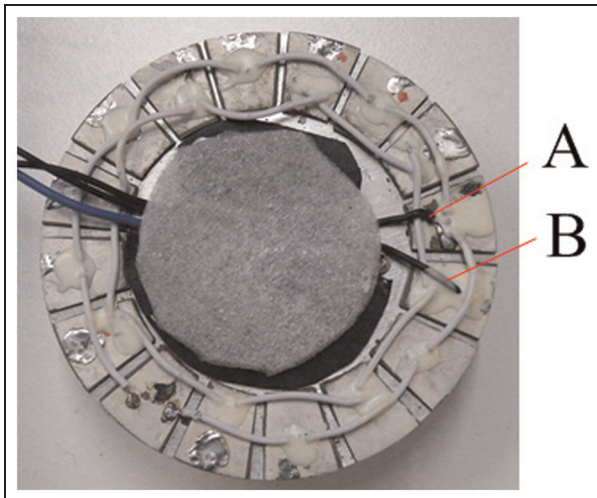


Figure 10. Prototype of the circular piezoelectric elements.

noted that the height distance becomes smaller with increasing the weight of the rotor. In the same manner, the levitation characteristics of stator II can also be experimentally obtained by applying a voltage of 260 V at frequency of 49.77 kHz. Figure 18 shows that the measured levitation distances are plotted against the rotor weight per unit area on the acoustic radiation surface. For the presented noncontact spherical bearing with bowl-shaped stator, the levitated weight per unit area is defined as

$$f = \frac{F}{2\pi R_1^2} \quad (14)$$

where F is the weight of levitated rotor and R_1 is internal radius of the bowl-shaped stator.

Figure 18 also permits the calculation of the levitation rigidity, defined as the ratio of the change of the

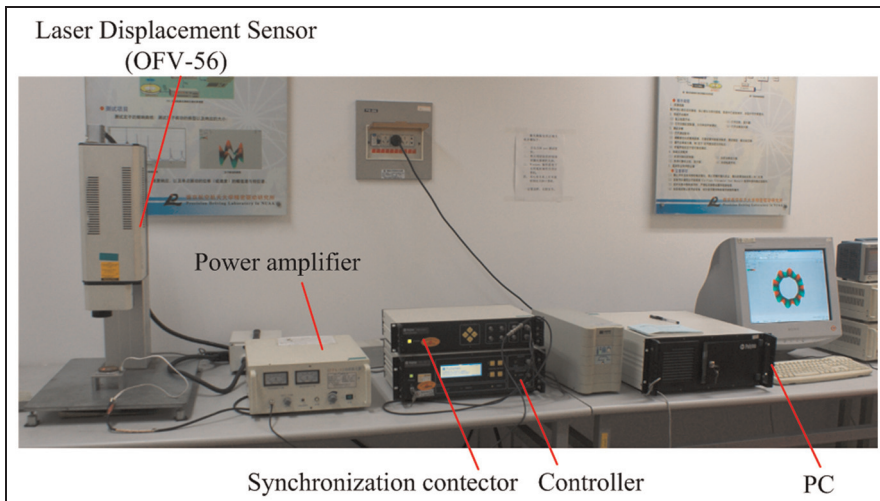


Figure 11. Laser Doppler Measurement System (PSV-300F-B).

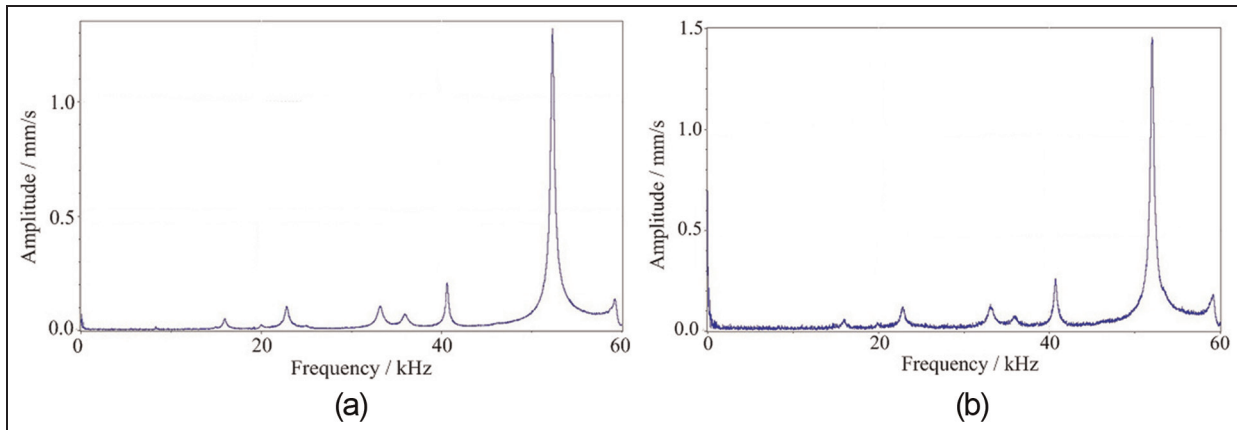


Figure 12. Frequency response curves of the stator using the optimal parameters: (a) applying voltage signals to group A and (b) applying voltage signals to group B.

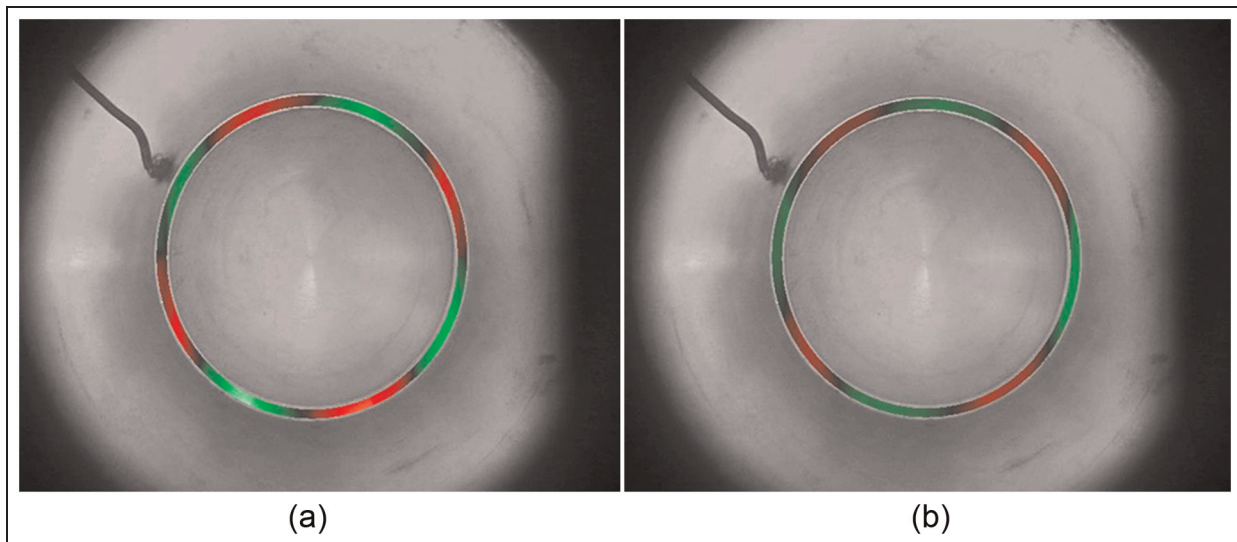


Figure 13. Displacement response in the axial direction: (a) Mode A and (b) Mode B.

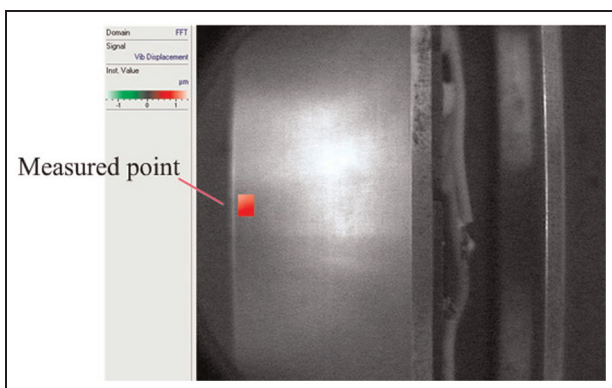


Figure 14. Radial displacement response.

rotor's weight per unit area to the rotor's levitation distance. It is found that stator I has higher levitation

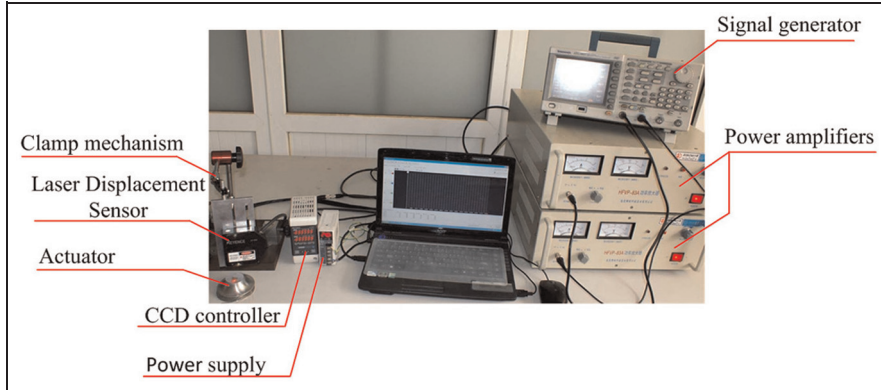
rigidity than stator II. Moreover, better levitation ability is obtained for stator I, and only about 26 kgf/m² arrive to the levitation limit of stator II.

The spherical rotor of 44 g, that is, the levitated weight per unit area of 19.4 kgf/m², is used to measure levitation distance with different applied voltages on the piezoelectric elements of stators I and II. In this case, the exciting voltages at their working frequencies are applied to stators I and II, respectively (see Table 3). As shown in Figure 19, larger levitation distance is obtained due to high voltages. It denotes that the levitation characteristics can be changed easily by controlling the applied voltages.

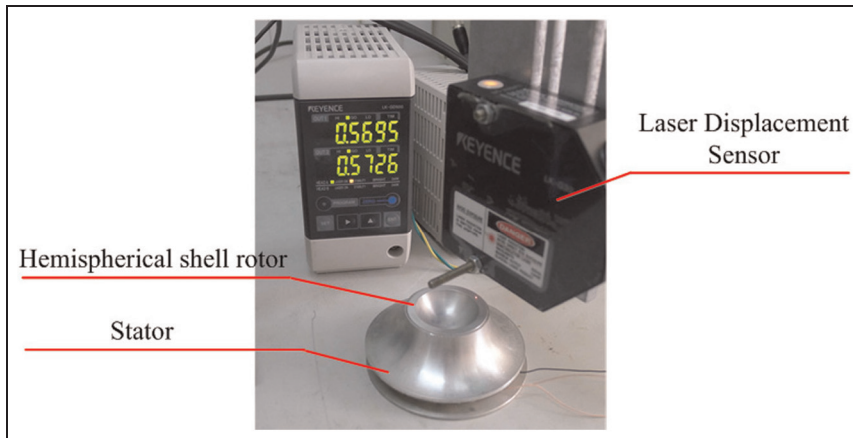
After the levitation distances are obtained, the theoretical levitation forces with different voltages can be figured out, which are compared with real force (0.44 N). We use the following equation for the radiation pressure in squeeze film levitation (Ueha et al., 2000)

Table 3. Measured modal response of stators using initial and optimal parameters.

Modal response	B_4 mode frequency (kHz)	Axial amplitude (μm)	Radial amplitude (μm)
Using initial parameters (stator II)	49.77	0.3	0.4
Using optimal parameters (stator I)	52.06	0.6	1.2

**Figure 15.** Measurement system of levitation characteristics.

CCD: charge-coupled device.

**Figure 16.** Detected hemispherical rotor.

$$\prod = \frac{1 + \gamma}{4} \rho_0 c^2 \frac{a_0^2}{h^2} \quad (15)$$

where γ represents specific heat ratio, ρ_0 is the air density, c is the sound speed, a_0 is the vibration amplitude, and h is the distance between the stator and the rotor. The displacement response of the stator is calculated by finite element method (FEM) with different voltages. The theoretical levitation force can be obtained by integration on the acting surface of the rotor (Zhao and Wallaschek, 2011). As shown in Figure 20, the error range of the levitation force may be from 15.4% to 25.6%.

Rotary experiment

The rotary experiment of the noncontact ultrasonic motor is also based on Laser Displacement Sensor (Keyence LK-G30), as shown in Figure 21. In this

case, a copper silk is bonded on the spherical surface of the rotor along the longitude, in order to probe rotary displacement of the prototype. When a laser beam from LK-G30 irradiates on the surface of the rotating rotor, the recurrent displacement increment, which is presented as transient peak, can be observed due to the bonded copper silk. The measured serial displacement peaks denote the copper silk passes through laser beam again and again, as shown in Figure 22. It is noted that there are two peaks every rotation of 360° for the prototype. So the time, T_{pp} , between two peaks represents the rotation time of 180° and can be used to calculate the rotary speed of the prototype as follows

$$n = \frac{60}{2 \times T_{pp}} \quad (16)$$

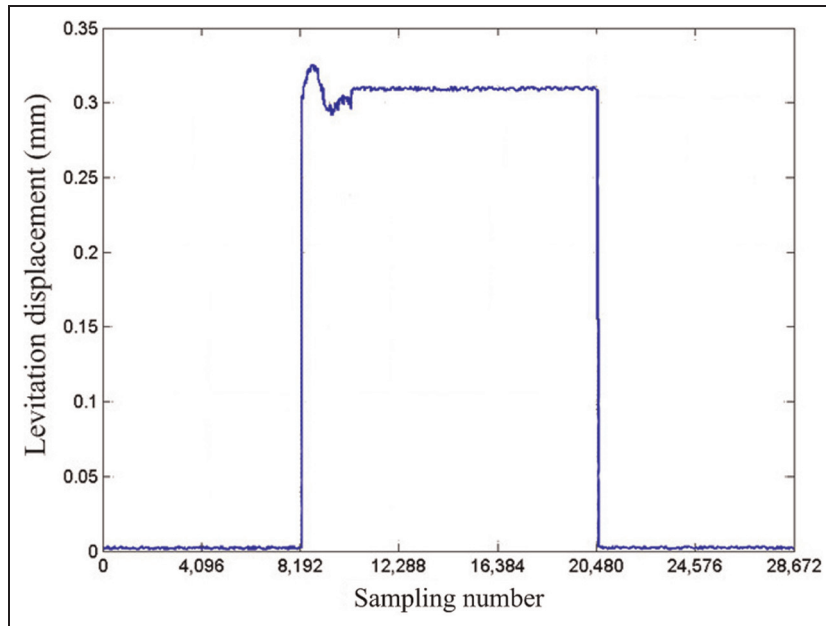


Figure 17. Measured levitation distance time history of spherical rotor by LK-G30.

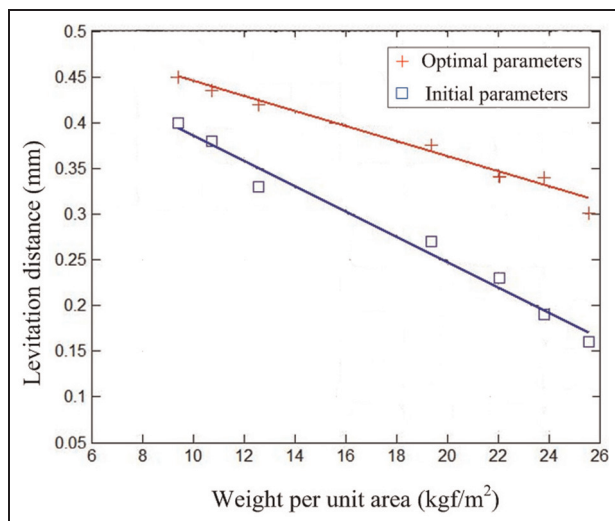


Figure 18. Levitation distance versus weight per unit area.

unit of which is revolutions per minute (rpm). Moreover, the consumed time between two peaks can be evaluated as follows

$$T_{pp} = m \times t_s \quad (17)$$

where m and t_s ($= 100$ ms) denote sampling number between two peaks and sampling period, respectively.

Figure 22 shows that the time history of the displacement is plotted against sampling number. In this experiment, a duralumin rotor of 24.32 g is levitated and driven to rotate by stator I. Also the recorded sampling number, m , between two peaks is about 280. So

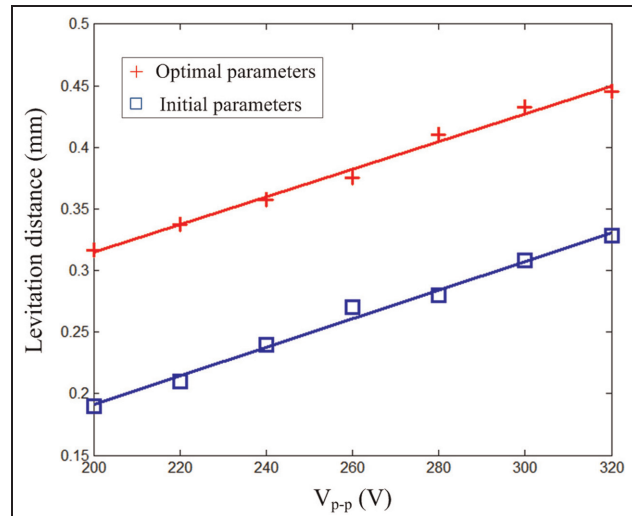


Figure 19. Levitation distance versus peak-to-peak value of applied voltages.

the prototype's revolution speed of about 1071.4 r/min was calculated using the above method

$$n = \frac{60}{2 \times (280 \times 100 \times 10^{-6})} \approx 1071.4 \text{ r/min}$$

Figure 23 shows the revolution speed of the rotors with different weights. In this case, the voltages of 400 V_{p-p} at frequencies of 52.06 and 49.77 kHz are applied to stators I and II, respectively. A maximal rotary speed of 1182 r/min was obtained for stator I, while only 230 r/min was obtained for stator II. As the stator based on optimal parameters has better vibration response, that is, larger displacement can be obtained with the same

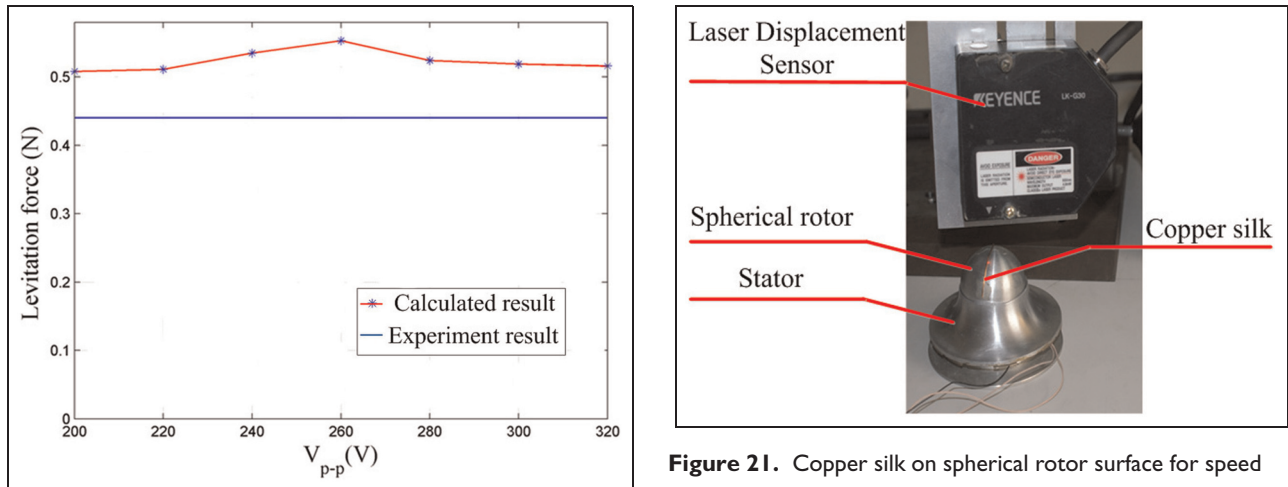


Figure 20. Theoretical levitation forces compared with experimental levitation force.

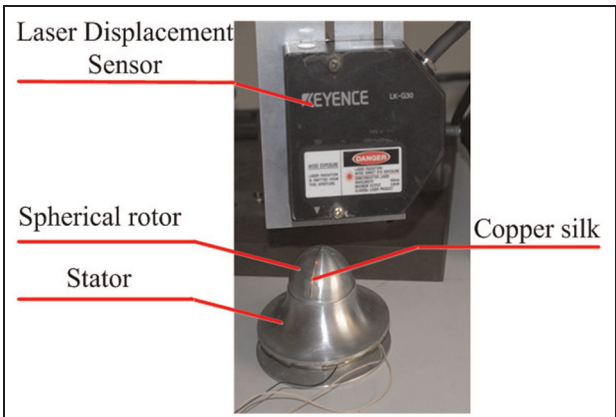


Figure 21. Copper silk on spherical rotor surface for speed measurement.

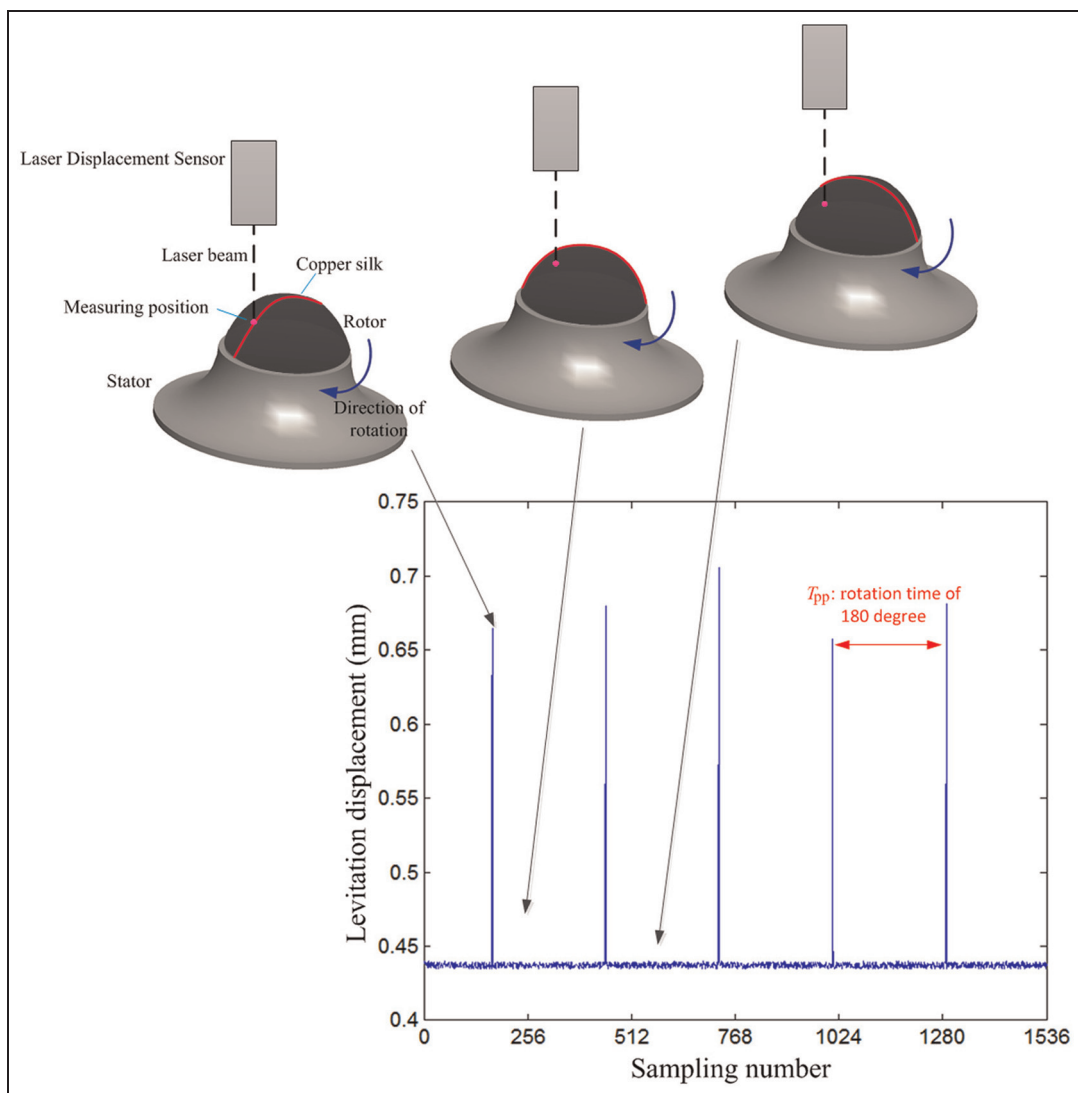


Figure 22. Measured displacement response of spherical rotor with bonded copper silk.

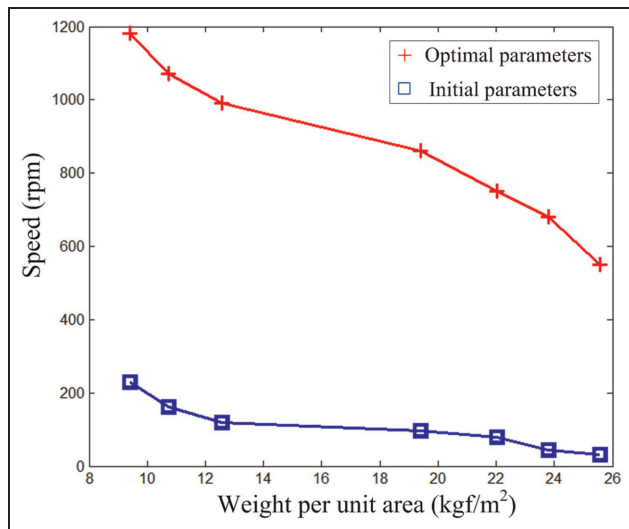


Figure 23. Rotary speed versus weight per unit area of levitation rotor.

excitation (see Table 3). It is well known that amplitude and frequency of vibrating surface have an effect on real acoustic radiation pressure. Then the stator applying optimal parameters can produce drive force and high speed is obtained.

As a matter of fact, the maximum speed of revolution is lower compared with the speed of traditional gyros. In the experiment, the phenomenon of heating exists in the prototype, which may be the main limit reason for the maximum speed of revolution. In addition, there is much energy vanishing from the bottom to the top of the stator. So, how to improve the structure of the prototype for the sake of enhancing the energy efficiency is an effective approach for increasing the maximum of revolution.

Conclusion

A noncontact ultrasonic motor with bowl-shaped stator was proposed and investigated for the levitated spherical rotor in this article. Using FEM, the parametric design for the bowl-shaped stator was carried out to obtain better vibration and levitation characteristics. On the basis of the calculated results, the prototypes with the stator using the initial and optimal parameters were manufactured. The experimental setup for the levitation and rotation characteristics is set up and the correspondent results denote that stator I using the optimal parameters obtains better vibration and levitation characteristics. Moreover, a maximum revolution speed of about 1071 r/min was measured for the prototype using stator I. In future research, an additional effort to increase the levitation rigidity and angular momentum is needed, in order to provide a potential design idea for the noncontact bearing and driving of suspended type inertial sensor.

Declaration of conflicting interests

The authors declare that there is no conflict of interest.

Funding

This study was supported by the National Basic Research Program of China (973 Program) (grant number 2011CB707202), National Natural Science Foundation of China (grant number 11174149), and Aviation Science Foundation (grant number 2011ZC52035).

References

- Chu B and Apfel E (1982) Acoustic radiation pressure produced by a beam of sound. *Journal of the Acoustical Society of America* 72(6): 1673–1687.
- Frazier RH, Gilison PJ and Oberbeck GA (1974) *Magnetic and Electric Suspensions*. The MIT Press, Cambridge, MA.
- Hashimoto Y, Koike Y and Ueha S (1995) Acoustic levitation of planar objects using a longitudinal vibration mode. *Journal of the Acoustical Society of Japan* 16(3): 189–192.
- Hashimoto Y, Koike Y and Ueha S (1998) Transporting objects without contact using flexural traveling waves. *Journal of the Acoustical Society of America* 103(6): 3230–3233.
- Higuchi T, Mizuno T and Aikawa N (1984) Experimental study of magnetic bearing control systems by an instrument with gyro mechanism. *Journal of the Japan Society of Precision Engineering* 50(9): 1439–1444.
- Hu JH, Nakamura K and Ueha S (1997) An analysis of a noncontact ultrasonic motor with an ultrasonically levitated rotor. *Ultrasonics* 35: 459–467.
- Hu JH, Nakamura K and Ueha S (2003) Stability analysis of an acoustically levitated disk. *IEEE Transactions on Ultrasonics, Ferroelectrics, and Frequency Control* 50(2): 117–127.
- Huxley AS, Nuttall JD and Witt DC (1987) The electrostatically suspended gyroscope—a review of mechanical design aspects. In: *International conference on the mechanical technology of inertial devices*, Newcastle-upon-Tyne, England, 7–9 April.
- Ide T, Friend J, Nakamura K, et al. (2005) A low-profile design for design for the noncontact ultrasonically levitated stage. *Japanese Journal of Applied Physics* 44(6B): 4662–4665.
- Ide T, Friend J, Nakamura K, et al. (2007) A noncontact linear bearing and actuator via ultrasonic levitation. *Sensors and Actuators A: Physical* 135: 740–747.
- Koyama D, Nakamura K and Ueha S (2007) A stator for a self-running ultrasonically-levitated sliding stage. *IEEE Transactions on Ultrasonics, Ferroelectrics, and Frequency Control* 54(11): 2337–2343.
- Lee C and Wang T (1993) Acoustic radiation pressure. *Journal of the Acoustical Society of America* 94(2): 1099–1109.
- Liu PK, Li J, Ding H, et al. (2009) Modeling and experimental study on near-field acoustic levitation by flexural mode. *IEEE Transactions on Ultrasonics, Ferroelectrics, and Frequency Control* 56(12): 2679–2685.
- Minikes A and Bucher I (2003) Noncontacting lateral transportation using gas squeeze film generated by flexural traveling waves—numerical analysis. *Journal of the Acoustical Society of America* 113(5): 2464–2473.

- Stolarski T (2010) Numerical modeling and experimental verification of compressible squeeze film pressure. *Tribology International* 43(12): 356–360.
- Stolarski T, Xue Y and Yoshimoto S (2011) Air journal bearing utilizing near field acoustic levitation stationary shaft case. *Proceedings of the Institution of Mechanical Engineers, Part J: Journal of Engineering Tribology* 225(3): 120–127.
- Titterton DH and Weston JL (1997) *Strap Down Inertial Navigation Technology*. Peter Peregrinus Ltd. London.
- Ueha S, Hashimoto Y and Koike Y (2000) Noncontact transportation using near-field acoustic levitation. *Ultrasonics* 38: 26–32.
- Yamayoshi Y, Hirose S, Sone S, et al. (1994) An analysis on the driving force and optimum frequency of a noncontact type ultrasonic motor. *Japanese Journal of Applied Physics Part I* 33(5B): 3081–3084.
- Yamazaki T, Hu JH and Ueha S (1996) Trial construction of a noncontact ultrasonic motor with an ultrasonically levitated rotor. *Japanese Journal of Applied Physics Part I* 35(5B): 3286–3288.
- Zhao CS (2010) *Ultrasonic Motors: Technologies and Applications*. Science Press, Springer-Verlag Berlin Heidelberg.
- Zhao S and Wallaschek J (2011) A standing wave acoustic levitation system for large planar objects. *Archive of Applied Mechanics* 81(2): 123–139.
- Zhao S and Wallaschek J (2012) An ultrasonic levitation journal bearing able to control spindle center position. *Mechanical Systems and Signal Processing*. Available at: <http://dx.doi.org/10.1016/j.ymssp.2012.05.006>